Journal Name

ARTICLE TYPE

Cite this: DOI: 10.1039/xxxxxxxxxx

NMR of Molecular Endofullerenes Dissolved in a Nematic Liquid Crystal

Karel Kouřil,*[a] Christopher Wickens,[a] Benno Meier,[a] Shamim Alom,[a] John Gräsvik,[a] Richard J. Whitby,[a] and Malcolm H. Levitt*[a]

Received Date
Accepted Date

DOI: 10.1039/xxxxxxxxxx

www.rsc.org/journalname

We report the NMR of the molecular endofullerenes $H_2@C_{60}$, $H_2O@C_{60}$ and $HF@C_{60}$ dissolved in the nematic liquid crystal N-(4-methoxybenzylidene)-4-butylaniline (MBBA). The ^{1}H NMR lines of H_2 and H_2O display a doublet splitting due to residual dipole-dipole coupling. The dipolar splitting depends on temperature in the nematic phase and vanishes above the nematic-isotropic phase transition. The ^{19}F spectrum of $HF@C_{60}$ dissolved in MBBA displays a doublet splitting in the nematic phase, with contributions from the ^{1}H-^{19}F dipole-dipole coupling and J-coupling. The phenomena are analyzed using a model in which the fullerene cages acquire a geometrical distortion, either through interaction with the liquid crystal environment, or through their interaction with the endohedral molecules. The distorted cages become partially oriented with respect to the liquid crystal director, and the endohedral molecules become partially oriented with respect to the distorted cages.

1 Introduction

Small molecules, such as H_2, H_2O and HF, can be fully encapsulated inside closed carbon cages, such as the fullerene C_{60} [1–3]. The resulting species are known as molecular endofullerenes, and denoted $H_2@C_{60}$, $H_2O@C_{60}$ and $HF@C_{60}$. These substances may be obtained as chemically pure black solids, in high yield and macroscopic quantities. A range of spectroscopic studies has established that the encapsulated molecules display complete rotational freedom inside the carbon cage [3,4]. Except for small frequency shifts, the spectroscopy of the encapsulated molecules resembles that observed for isolated guest molecules in the gas phase [3,5–9]. The endohedral molecules display rotational and translational quantization under cryogenic conditions, with a translation-rotation coupling observed under some circumstances [5,6,8–10]. Furthermore, the symmetrical molecular species H_2 and H_2O display spin-isomerism phenomena, with the slow conversion between the *ortho* and *para* spin isomers observed by infrared spectroscopy and by NMR [7,11,12]. At low temperatures the dielectric constant of $H_2O@C_{60}$ depends on the ratio of the *ortho* and *para* water spin isomers [13].

There is one qualitative difference between the quantum energy levels of the guest molecules in the gas phase and in the encapsulated state: Some of the rotational energy levels display a reduced degeneracy in the molecular endofullerenes. For example, neutron scattering has shown that the three-fold degeneracy of the $J = 1$ rotational ground state of *ortho*-H_2 is broken in solid $H_2@C_{60}$, in the cryogenic solid state [14]. An energy level splitting of the *ortho*-H_2O ground state is also observed in $H_2O@C_{60}$ [7,15,16]. Some energy level degeneracies are also lifted in $HF@C_{60}$ [3]. The lifting of degeneracies indicates a reduction in symmetry of the enclosing C_{60} cage. This symmetry reduction persists to room temperature as shown by the solid-state NMR of $H_2O@C_{60}$ [7,15] and $HF@C_{60}$ [3].

The electron paramagnetic resonance (EPR) spectra of the atomic endofullerenes $N@C_{60}$ and $N@C_{70}$ also display the signature of broken symmetry, when the endofullerenes are dissolved in anisotropic liquids [17,18]. The encapsulated nitrogen atom has three unpaired electrons, with a spin $S = 3/2$ ground state, and displays a triplet of very narrow EPR lines in isotropic solution, with the triplet splitting attributed to the hyperfine coupling between the electron spin and the nuclear spin $I = 1$ of the nitrogen-14 nucleus. When the species $N@C_{70}$ is dissolved in a nematic liquid crystal, each of the three EPR peaks splits into a further three components. This is attributed to a finite zero-field splitting for the electronic ground state in anisotropic phase, reflecting partial alignment of the anisotropic C_{70} cages by the nematic liquid crystal [17,18]. This is unsurprising, since C_{70} has an elongated geometry, and presents an anisotropic environment for the endohedral nitrogen atom.

More surprisingly, liquid crystal solutions of the atomic endofullerene $N@C_{60}$ also display EPR splittings due to a finite zero-field splitting [17,18]. Since isolated C_{60} cages have high icosahedral symmetry, under which the zero-field splitting should vanish, the

[a] School of Chemistry, University of Southampton, SO17 1BJ Southampton, UK. E-mail: k.kouril@soton.ac.uk, mhl@soton.ac.uk

existence of a finite zero-field splitting in these systems indicates a distortion of the C_{60} cage, either through an external mechanism (in which the interaction with the anisotropic liquid crystal environment slightly distorts the C_{60} cages), or through an internal mechanism, in which Jahn-Teller distortion[19] of the $N@C_{60}$ system occurs on a single-molecule level, with the liquid crystal imposing a partial alignment on the spontaneously distorted cages.

In this paper we show that analogous phenomena are observed for the molecular endofullerenes $H_2@C_{60}$, $H_2O@C_{60}$ and $HF@C_{60}$, dissolved in a nematic liquid crystal. In this case the breaking of C_{60} symmetry and partial alignment of the endohedral molecules is revealed by NMR spectroscopy. The ^{1}H NMR of $H_2@C_{60}$ and $H_2O@C_{60}$ in nematic liquid crystal solution display splittings due to residual dipolar couplings between the protons of the endohedral molecule. The ^{19}F NMR of $HF@C_{60}$ in anisotropic solution displays a splitting from the ^{1}H-^{19}F coupling, with a strong contribution from the residual dipole-dipole coupling. Temperature-dependent chemical shifts are observed, and are interpreted in terms of magnetic susceptibility and residual chemical shift anisotropy effects.

2 Experimental

2.1 Samples

The endofullerenes were prepared by molecular surgical techniques[3,4]. MBBA (N-(4-methoxybenzylidene)-4-butylaniline) was used as purchased from Sigma-Aldrich (UK).

The starting materials were as follows: 5 mg of $H_2O@C_{60}$ (purified by HPLC and sublimation, H_2O incorporation 78%); 3.5 mg of $H_2@C_{60}$ (purified by HPLC but not sublimed, H_2 incorporation 67%); 2 mg of $HF@C_{60}$ (purified by HPLC and sublimation, HF incorporation 34%). The purified endofullerenes were mixed with 1 ml of MBBA and left in an oven for approximately 3 days at 70°C. The resulting brown solutions were allowed to cool to room temperature, centrifuged to separate the undissolved solids, and the liquids pipetted into 5 mm NMR tubes. The precise concentrations of the dissolved endofullerenes are not known.

The nematic-to-isotropic phase transition of pure MBBA occurs at 320 K[20,21]. The endofullerene solutions in MBBA display somewhat depressed phase transition temperatures, as shown below.

2.2 NMR

^{1}H and ^{19}F NMR experiments were performed on a 500 MHz Bruker Avance III spectrometers using a standard high-resolution 5 mm NMR probes, ^{13}C experiments experiments were performed on a 300 MHz Bruker Avance III spectrometer using a 10 mm probe. ^{1}H spectra of $H_2@C_{60}$ and $H_2O@C_{60}$ were measured using a standard pulse–acquire sequence in the isotropic phase. In the nematic phase the ^{1}H spectra of $H_2@C_{60}$ and $H_2O@C_{60}$ were measured using a "perfect echo" sequence[22–24], with an echo interval $\tau = 10$ ms, to suppress the broad background signal of the MBBA liquid crystal (see below).

The ^{19}F and ^{1}H spectra of $HF@C_{60}$ and ^{13}C spectra of $H_2O@C_{60}$ were measured using a standard pulse–acquire sequence.

3 Results

3.1 $H_2O@C_{60}$ in MBBA

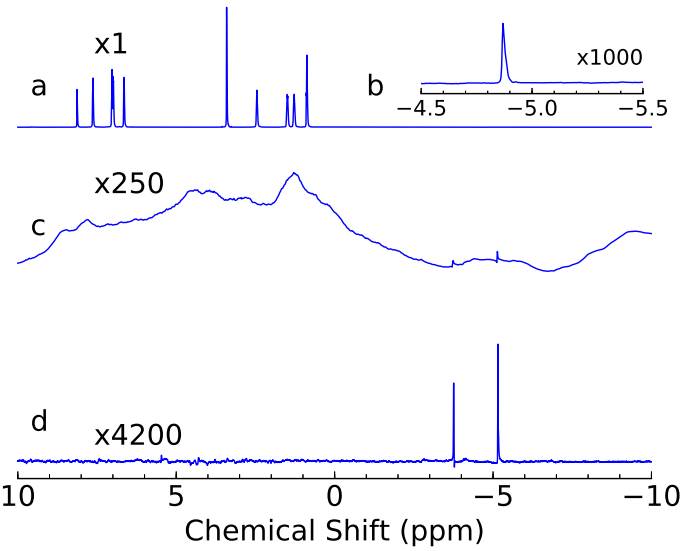

Fig. 1 ^{1}H NMR spectra of $H_2O@C_{60}$ dissolved in MBBA. (a) Spectrum recorded in isotropic phase ($T = 325$ K) showing the narrow lines of the MBBA solvent. (b) Detail of the isotropic spectrum (intensity multiplied approximately by 1000) showing the $H_2O@C_{60}$ line at $\delta = -4.9$ ppm. (c) Spectrum recorded in the nematic phase ($T = 298$ K) using a single $\pi/2$ pulse. The spectrum is dominated by the unresolved broad background from the MBBA solvent (intensity multiplied approximately by 250). (d) Spectrum recorded in the nematic phase ($T = 298$ K) using a perfect echo sequence with $\tau = 10$ ms (intensity multiplied approximately by 4200). The MBBA background is suppressed allowing clear observation of the $H_2O@C_{60}$ doublet.

The ^{1}H spectra of $H_2O@C_{60}$ dissolved in MBBA taken at two different temperatures are shown in figure 1. At high temperature, in the isotropic phase, resolved peaks from the MBBA are observed, as well as a small narrow peak from the $H_2O@C_{60}$ solute at -4.9 ppm relative to tetramethylsilane (TMS) (Fig. 1(a,b)). At lower temperature, in the nematic phase of MBBA, the liquid crystal peaks become very broad due to the complex network of ^{1}H-^{1}H dipole-dipole couplings, almost obscuring the endofullerene signals (Fig. 1(c)).

The broad MBBA signals were suppressed by using the "perfect echo" sequence[22–24]

$$90_x - \tau/2 - 180_y - \tau/2 - 90_y - \tau/2 - 180_x - \tau/2 - \text{acquire} \qquad (1)$$

with an echo interval $\tau = 10$ ms. This pulse sequence induces an accurate refocusing of dipolar coupling and J-coupling effects, but only in the case of isolated spin-1/2 pairs. The "perfect echo" dipolar refocusing fails for the complex dipolar-coupled spin network of the liquid crystal molecules, leading to a strong suppression of the liquid crystal background signals, relative to that of the endofullerene solute, as shown in Fig. 1(d).

The ^{1}H spectra of $H_2O@C_{60}$ dissolved in MBBA, in the nematic and isotropic phases, are shown as a function of temperature in figure 2. The spectra display a temperature-dependent line splitting in the nematic phase. The splitting decreases with increas-

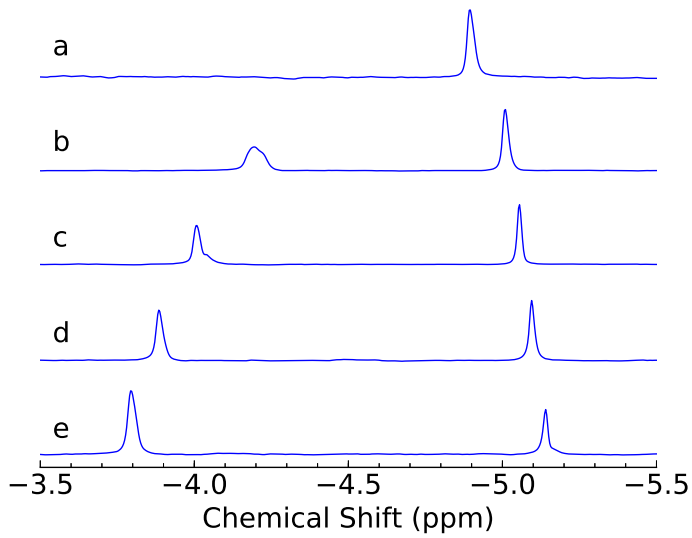

Fig. 2 ^{1}H NMR spectra of $H_2O@C_{60}$ dissolved in MBBA liquid crystal recorded at several temperatures (a: $T = 316$ K, b: $T = 312$ K, c: $T = 308$ K, d: $T = 304$ K, e: $T = 300$ K). Spectrum (a) was recorded in the isotropic phase using a single pulse excitation and shows a single peak at -4.9ppm. Spectra (b-e) were obtained using a perfect echo sequence with $\tau = 10$ ms.

ing temperature until it abruptly vanishes at the nematic-isotropic phase transition at $T = 314$ K (see figure 3). No resolved lines could be observed within approximately ± 1 K of the nematic-to-isotropic transition temperature.

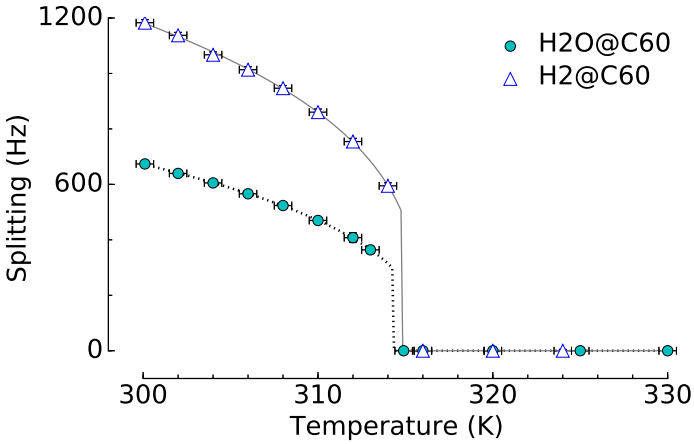

Fig. 3 Temperature dependencies of the dipolar splittings of $H_2@C_{60}$ and $H_2O@C_{60}$ dissolved in MBBA. The lines are fits to equation 15 (see text).

The mean chemical shift of the doublet also changes with temperature (see figure 4). The shift decreases with increasing temperature in the nematic phase, has a discontinuous jump of approximately 0.25 ppm at the transition temperature and displays a weak linear increase with temperature in the isotropic phase.

As shown in Figure 2, the less shielded peak is consistently broader than the more shielded peak at the same temperature, in the nematic phase. This differential linewidth effect is not completely understood, but may be due to a distribution of temperatures or order parameters in the sample. The temperature dependence of the chemical shift and the dipolar splitting leads to frequency shifts with the same sign for the less-shielded peak, but opposite sign for the more-shielded peak. A temperature distribution in the sample therefore broadens the less-shielded peak more than the more-shielded peak.

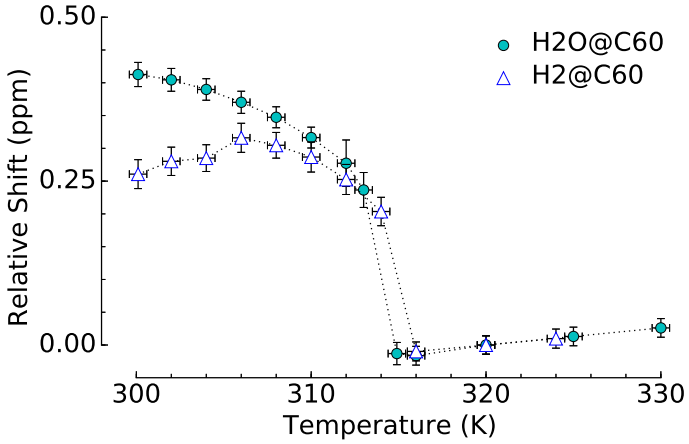

Fig. 4 Temperature-dependence of ^{1}H chemical shifts for $H_2@C_{60}$ and $H_2O@C_{60}$ in MBBA solution. The plotted values are chemical shifts relative to those observed for the same solutions in isotropic phase at $T = 320$ K (-1.53 ppm relative to TMS for $H_2@C_{60}$, and -4.88 ppm relative to TMS for $H_2O@C_{60}$).

The ^{13}C spectrum of $H_2O@C_{60}$ dissolved in nematic MBBA at room temperature is shown in figure 5. The spectrum consists of two narrow ^{13}C peaks on a broad MBBA background. The less shielded ^{13}C peak comes from the H_2O filled cages and the more shielded one from the empty cages. The chemical shift difference is ~ 0.11 ppm, close to that observed in (isotropic) toluene solution[4].

3.2 $H_2@C_{60}$ in MBBA

The spectrum of $H_2@C_{60}$ in MBBA shows analogous behavior to that of $H_2O@C_{60}$. The ^{1}H spectra recorded at several temperatures are shown in figure 6. The relatively low signal-to-noise ratio of these spectra is attributed to low incorporation and purity of the $H_2@C_{60}$ sample. As in the case of $H_2O@C_{60}$, the dipolar splitting of $H_2@C_{60}$ in the nematic liquid crystal solution decreases with increasing temperature, collapsing at the nematic-to-isotropic phase transition ($T = 315$ K, see figure 3). No well resolved lines were observed within approximately 1 K of the transition temperature.

The chemical shift of $H_2@C_{60}$ in MBBA shows a non-monotonic temperature dependence in the nematic phase (see Figure 4). There is a jump in the chemical shift at the phase transition, followed by an approximately linear increase upon further increase in temperature. The chemical shift behaviour of $H_2@C_{60}$ in MBBA is very similar to that observed for $H_2O@C_{60}$, except for temperatures well below the phase transition.

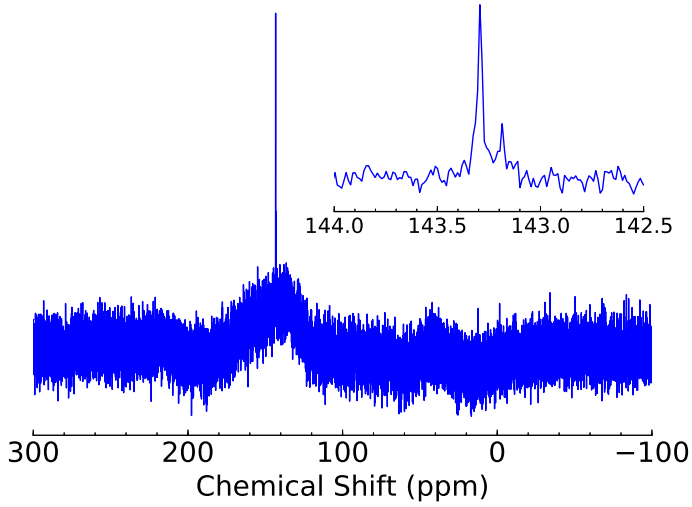

Fig. 5 ^{13}C NMR spectrum of $H_2O@C_{60}$ dissolved in MBBA liquid crystal recorded at room temperature (nematic phase) using a pulse–acquire sequence, without proton decoupling. The inset shows ^{13}C signals of $H_2O@C_{60}$ and C_{60} cages at 143.29 ppm and 143.18 ppm respectively.

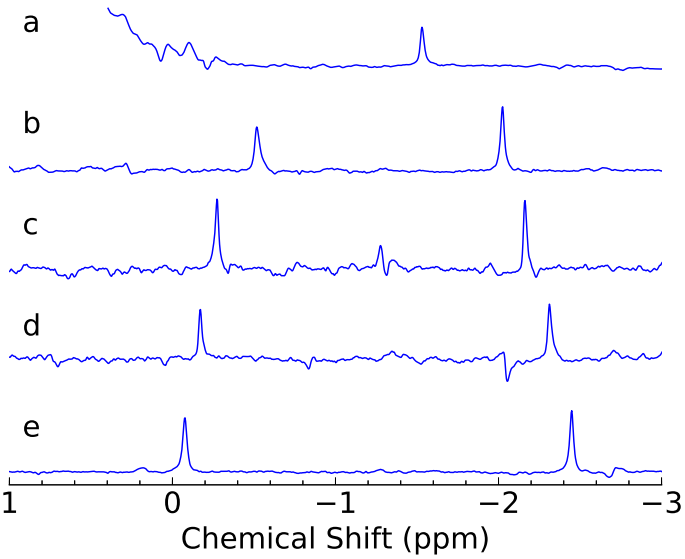

Fig. 6 ^{1}H NMR spectra of $H_2@C_{60}$ dissolved in MBBA, recorded at several temperatures: (a) $T = 316$ K; (b) $T = 312$ K; (c) $T = 308$ K; (d) $T = 304$ K; (e) $T = 300$ K. Spectrum (a) was recorded in the isotropic phase using a single pulse excitation and shows a single peak at -1.5ppm. The intense MBBA signals have been truncated. Spectra (b-e) were observed in the nematic phase using a perfect echo sequence to suppress the liquid crystal background.

3.3 HF@C_{60} in MBBA

The room temperature ^{19}F spectrum of $HF@C_{60}$ dissolved in nematic MBBA is shown in figure 7. The spectrum consists of a doublet centered at -219.1 ppm with a splitting of 2710 Hz. The observed splitting is much larger than the 506 Hz $^{19}F-{}^1H$ J-coupling observed in isotropic toluene solution[3]. A temperature-dependence was not recorded for this sample, due to equipment constraints.

The ^{1}H spectra of $HF@C_{60}$ could not be observed in the nematic phase due to the too strong background signal from the MBBA. At 325 K, in the isotropic phase, a weak $HF@C_{60}$ signal was observed in the ^{1}H spectrum. The signal consisted of a doublet centered at -2.8 ppm (relative to TMS) with splitting $J_{HF} = 506$ Hz.

4 Analysis

Anisotropic nuclear spin interactions are averaged to a small but finite value in the anisotropic phase. There are two classes of relevant interactions in the systems studied here: (1) The magnetic dipole-dipole interactions between the pair of protons in $H_2@C_{60}$ and $H_2O@C_{60}$, and between the ^{1}H and ^{19}F nuclei in $HF@C_{60}$. The motional average of these dipole-dipole couplings in anisotropic phase is called the residual dipolar coupling (RDC)[25–28]. The RDC is entirely responsible for the doublet splittings of the ^{1}H spectra for $H_2@C_{60}$ and $H_2O@C_{60}$ in anisotropic phase. In the case of $HF@C_{60}$, on the other hand, the spin system is heteronuclear, so the doublet splitting is generated by a combination of the $^1H-{}^{19}F$ RDC and J-coupling. (2) The chemical shift anisotropy (CSA) interaction has a non-vanishing average in anisotropic phase, which is known as the residual CSA (RCSA)[26,29]. The RCSA contributes to the peak frequencies in anisotropic phase.

The peak frequencies in anisotropic phase are also strongly influenced by the magnetic susceptibility of the liquid crystal solvent, which is strongly temperature-dependent in the vicinity of the phase transition[30–32].

4.1 Residual Dipolar Couplings

4.1.1 Homonuclear splittings.

The spectral splittings $\Delta\omega_{HH}$ observed in the ^{1}H spectra of $H_2@C_{60}$ and $H_2O@C_{60}$ in anisotropic phase are due to the residual dipole-dipole couplings (RDC), according to the equation[33]

$$\Delta\omega_{HH} = 3\omega_{HH}^{RDC} \tag{2}$$

The RDC is given by

$$\omega_{HH}^{RDC} = \kappa_Q b_{HH} S_{HH}^2 \tag{3}$$

and κ_Q is a quantum delocalization factor, discussed below. The dipolar coupling constant for the magnetic interaction between two localized protons at an internuclear distance r_{HH} is given by

$$b_{HH} = -\frac{\mu_0}{4\pi}\gamma_H^2 \hbar r_{HH}^{-3} \tag{4}$$

where γ_H is the ^{1}H magnetogyric ratio. The order parameter S_{HH}^2 for the $^1H-{}^1H$ dipole-dipole interaction is defined as follows

$$S_{HH}^2 = \langle d_{00}^2(\beta_{PL}^{HH})\rangle \tag{5}$$

where d^2 is the second-rank reduced Wigner rotation matrix[34], with central element $d_{00}^2(\beta_{PL}) = (3\cos^2\beta_{PL} - 1)/2$, and β_{PL}^{HH} is the instantaneous angle between the principal axis of the $^1H-{}^1H$ dipole-dipole interaction (parallel to the $^1H-{}^1H$ internuclear vector) and the z-axis of the laboratory frame (defined to be along

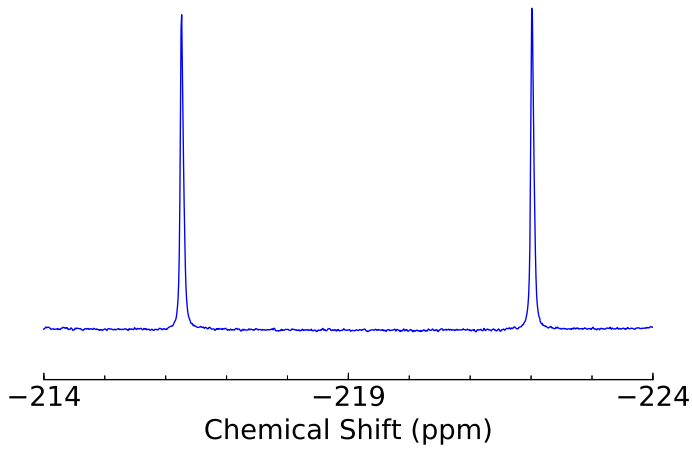

Fig. 7 ^{19}F NMR spectrum of HF@C_{60} dissolved in MBBA liquid crystal recorded at room temperature using the pulse-acquire sequence. The spectrum consists of a doublet with splitting 2710 Hz, much larger than the scalar coupling $J_{HF} = 506$ Hz.

the external magnetic field). This equation assumes that the dipolar interactions fluctuate on a timescale that is short compared to the magnitude of the anisotropic spin Hamiltonian. The angular brackets denote a local ensemble average (equivalent to a long-time average, under the ergodic hypothesis).

The factor κ_Q in equation 3 takes into account the quantum delocalization of the nuclear wavefunctions. This factor arises because the dipole-dipole coupling between nuclei in quantum rotor systems is reduced by the angular spread of the delocalized spatial wavefunction[35–38]. For example, in the case of H_2, the NMR signals originate from the *ortho*-H_2 spin isomer. The dipole-dipole coupling in the *ortho*-hydrogen ground state ($J = 1$) is reduced with respect to the point-nucleus model by a factor $\kappa_Q = 2/5$, which may be derived analytically from the functional form of the spatial nuclear wavefunction[35–38]. In principle, a larger value of κ_Q may exist (eventually approaching $\kappa_Q = 1$) when the angular part of the nuclear wavefunction is localized, as can occur in the presence of a strongly anisotropic rotational potential, which mixes together many rotational states. However, neutron diffraction and infrared measurements of both H_2@C_{60} and H_2O@C_{60} have shown that such rotational state mixing is limited in scope in these systems, even at relatively high temperatures. For example, the energy level structure of C_{60}-encapsulated H_2 is similar to that observed in the gas phase, where the energy splitting between the $J = 1$ and $J = 3$ states is equivalent to 876 Kelvin[5,6,10,14]. This implies that the excited rotational states of *ortho*-hydrogen are weakly populated, even at room temperature. The quantum delocalization factor κ_Q is therefore likely to be close to its ground state value of 2/5, although at present, a robust theory of κ_Q has not been described for either H_2@C_{60} or H_2O@C_{60}, at arbitrary temperature. In any case, the large uncertainty in the value of κ_Q is masked by equally large uncertainties in the other anisotropic system parameters, as discussed below.

In the case of H_2@C_{60}, the assumed dipole-dipole coupling parameters are $r_{HH} = 74.1$ pm, $b_{HH} = -2\pi \times 295$ kHz, $\kappa_Q = 2/5$. The observed splitting $|\Delta\omega_{HH}| = 2\pi \times 1180$ Hz leads to an estimated order parameter for H_2@C_{60} in MBBA of $|S^2_{HH}| = 0.0033$ at a temperature of 300 Kelvin.

In the case of H_2O@C_{60}, the assumed dipole-dipole coupling parameters are $r_{HH} = 152$ ppm, $b_{HH} = -2\pi \times 34.5$ kHz, $\kappa_Q = 2/5$. The observed splitting $|\Delta\omega_{HH}| = 2\pi \times 670$ Hz leads to an estimated order parameter for H_2O@C_{60} in MBBA of $|S^2_{HH}| = 0.016$ at a temperature of 300 Kelvin.

4.1.2 Heteronuclear splitting in HF@C_{60}.

The ^{19}F spectral splitting for HF@C_{60} has three contributions: the isotropic $^1H - ^{19}F$ J-coupling, the $^1H - ^{19}F$ dipole-dipole coupling and the J-coupling anisotropy. For simplicity, the J-anisotropy contribution is neglected. The spectral splitting in both the ^{1}H and the ^{19}F spectrum is given by

$$\Delta\omega_{HF} = 2\pi J_{HF} + 2\omega^{RDC}_{HF} \tag{6}$$

where the RDC is given by

$$\omega^{RDC}_{HF} = \kappa_Q b_{HF} S^2_{HF} \tag{7}$$

The $^1H - ^{19}F$ dipolar coupling constant is given by

$$b_{HF} = -\frac{\mu_0}{4\pi}\gamma_H \gamma_F \hbar r^{-3}_{HF} \tag{8}$$

The assumed dipole-dipole coupling parameters are $r_{HF} = 91.7$ pm, $b_{HF} = -2\pi \times 147$ kHz, $\kappa_Q = 2/5$. The 2710 Hz splitting for the ^{19}F spectrum of HF@C_{60} in nematic phase therefore corresponds to a HF dipole-dipole order parameter $|S^2_{HF}|$ of either 0.027 or 0.019, depending on the assumed relative sign of the dipole-dipole and J-coupling terms.

These results indicate that the dipolar order parameters for H_2O@C_{60} and HF@C_{60} in MBBA are both a few percent, while the order parameter for H_2@C_{60} is significantly smaller.

4.1.3 Physical model.

The NMR observations show that the endohedral molecules experience a partial orientation with respect to the magnetic field in nematic phase. This effect could arise in two ways: *1. Direct mechanism.* The endohedral molecules interact directly with the oriented liquid crystal molecules through the walls of the carbon cage. Since the liquid crystals are partially oriented along their director, the endohedral molecules also become oriented. *2. Indirect mechanism.* The icosahedral C_{60} cages are slightly distorted, and display a lowered symmetry. This distortion could either be intrinsic to the endofullerene, or generated by the liquid crystal environment. The distorted cages become partially oriented through interactions with the liquid crystal environment, and the endohedral molecules become partially oriented through interaction with the distorted cages. Since there is abundant evidence that the C_{60} cages of molecular endofullerenes exhibit a broken symmetry[7,8,14–16], we favor the indirect mechanism (2).

Define a series of reference frames as follows: Laboratory frame L, liquid crystal director frame D, fullerene cage frame C, molecular frame M and principal axis frame P^Λ of a tensorial spin interaction Λ. The z-axis of the laboratory frame L is defined to be parallel to the external magnetic field. The z-axis of the frame

D is defined to be parallel to the liquid crystal director. We assume that the liquid crystal is nematic and has rotational symmetry around the director axis. For simplicity the cage distortion is assumed to be uniaxial, defining the z-axis of frame C to be along the unique distortion axis. The axes of frame M have a fixed orientation with respect to the endohedral molecule. In the case of $H_2@C_{60}$ and $HF@C_{60}$, the z-axis of frame M is defined to be parallel to the internuclear vector. In the case of $H_2O@C_{60}$, the z-axis of frame M bisects the H-O-H angle. The z-axis of frame P^Λ is along the principal axis of a spin interaction tensor Λ (for example, a dipole-dipole coupling).

The instantaneous relative orientation of two reference frames F and G is expressed using the Euler angle triplet $\Omega_{FG} = \{\alpha_{FG}, \beta_{FG}, \gamma_{FG}\}$, which implies that frame F may be brought into coincidence with frame G by subjecting the axes of frame F to the following sequence of rotations: (1) A rotation through α_{FG} about the z-axis of frame G; A rotation through β_{FG} about the y-axis of frame G; (3) A rotation through γ_{FG} about the z-axis of frame G[34].

Assuming that the statistical distributions in all Euler angle sets are uncorrelated, the order parameter for a uniaxial intramolecular interaction Λ is given by

$$\begin{aligned} S^2_\Lambda &= \langle D^2_{00}(\Omega^\Lambda_{PL})\rangle \\ &= \sum_{m',m'',m'''=-2}^{+2} D^2_{0m'}(\Omega^\Lambda_{PM})\langle D^2_{m'm''}(\Omega_{MC})\rangle \times \\ &\qquad \langle D^2_{m''m'''}(\Omega_{CD})\rangle\langle D^2_{m'''0}(\Omega_{DL})\rangle \end{aligned} \quad (9)$$

Where $D^2_{mm'}(\Omega_{FG}) = e^{-im\alpha_{FG}} d^2_{mm'}(\beta_{FG}) e^{-im'\gamma_{FG}}$ are Wigner rotation matrices[34].

Assume that the orientation tensor of the molecule in the distorted cage is uniaxial, the liquid phase is nematic, that the director is parallel to the magnetic field, and neglect director fluctuations. In this case, $\beta_{DL} = 0$, all $m' \neq 0$, $m'' \neq 0$ and $m''' \neq 0$ averages vanish, and we get

$$S^2_\Lambda = d^2_{00}(\beta^\Lambda_{PM}) S^2_{MC} S^2_{CD} \quad (10)$$

where S^2_{MC} is the order parameter for the molecule with respect to the distorted cage

$$S^2_{MC} = \langle d^2_{00}(\beta_{MC})\rangle \quad (11)$$

and S^2_{CD} is the order parameter for the cage with respect to the liquid crystal director

$$S^2_{CD} = \langle d^2_{00}(\beta_{CD})\rangle \quad (12)$$

In the case of the diatomics H_2 and HF, the z-axis of the molecular frame is parallel to the internuclear vector, so that $\beta^{HH}_{PM} = \beta^{HF}_{PM} = 0$. The dipolar order parameter in these systems is therefore given by

$$\begin{aligned} S^2_{HH}(H_2@C_{60}) &= S^2_{MC}(H_2@C_{60}) S^2_{CD}(H_2@C_{60}) \\ S^2_{HF}(HF@C_{60}) &= S^2_{MC}(HF@C_{60}) S^2_{CD}(HF@C_{60}) \end{aligned} \quad (13)$$

The case of $H_2O@C_{60}$ is more complex, since the H_2O molecule is not axially symmetric. For the sake of simplicity, we assume that the orientation tensor of the H_2O molecule is axially symmetric around the electric dipole moment of the H_2O molecule. In this case, the angle between the $^1H - {}^1H$ internuclear vector and the z-axis of the molecular frame is $\beta^{HH}_{PM} = \pi/2$, which leads to

$$S^2_{HH}(H_2O@C_{60}) = -\frac{1}{2} S^2_{MC}(H_2O@C_{60}) S^2_{CD}(H_2O@C_{60}) \quad (14)$$

All order parameters in Eqs. 13 and 14 are the product of an order parameter for the partial orientation of the endohedral molecule with respect to the distorted C_{60} cage, and an order parameter for the partial orientation of the distorted cage with respect to the liquid crystal director. The observed temperature-dependence of the dipolar splitting, as shown in Figure 3, has a similar form to the order parameter for the liquid crystal molecules themselves[20,21], and is likely to derive predominantly from the temperature dependence of the order parameter S^2_{CD}, which describes the partial orientation of the distorted cages with respect to the liquid crystal director. The order parameter S^2_{MC}, which describes the orientation of the endohedral molecules with respect to the distorted cage, is expected to have a relatively mild temperature-dependence.

Figure 3 shows fits of the dipolar splittings to the Haller equation[20], which describes the typical temperature dependence of order parameters in a liquid crystal below the nematic-to-isotropic transition temperature T_{NI}

$$\Delta\omega(T) = \Delta\omega(0)\left(1 - \frac{T}{T^*}\right)^\gamma; \quad T \leq T_{NI} \quad (15)$$

The splitting $\Delta\omega(T)$ vanishes for $T > T_{NI}$. In general, the temperature origin T^* is slightly above T_{NI}. For $H_2@C_{60}$, the fitted parameters are $\Delta\omega(0) = 2\pi \times 3.10$ kHz, $T_{NI} = 314.8$ K, $T^* = 315.8$ K, $\gamma = 0.32$. For $H_2O@C_{60}$, the fitted parameters are $\Delta\omega(0) = 2\pi \times 2.00$ kHz, $T_{NI} = 314.3$ K, $T^* = 316.0$ K, $\gamma = 0.37$. The fitted exponents are larger than the typical parameter for MBBA, which is $\gamma \sim 0.2$[20]. The deviation may be due to the temperature-dependence of the order parameter for orientation of the endohedral molecule in the distorted cages, S^2_{MC}.

4.2 ^{1}H Chemical Shifts

The temperature-dependent ^1H chemical shifts for $H_2@C_{60}$ and $H_2O@C_{60}$ in MBBA solution are plotted in Figure 4. The plotted points show the difference between the chemical shift observed at a given temperature and the chemical shift of the same solution in isotropic phase at 320 K. This presentation isolates the influence

of the anisotropic ordering on the chemical shift. The behavior of the two compounds is qualitatively similar for much of the range, although with a significant divergence at temperatures well below the phase transition.

There are three possible contributions to the observed chemical shift changes:

1. Magnetic susceptibility. The magnetic susceptibility of liquid crystals is strongly temperature-dependent at temperatures below the nematic-to-isotropic phase transition, with a discontinuity at the transition itself[30–32]. These susceptibility changes give rise to a temperature-dependent chemical shift for ^{3}He dissolved in liquid crystals[39]. The reported shifts are of the order of ~ 0.2 ppm – of similar magnitude to the chemical shift changes observed here.

2. Intramolecular RCSA. Partial orientation of the endohedral molecules with respect to the magnetic field generates a RCSA contribution, in direct analogy to the RDC interaction discussed above. This contribution depends on the orientation of the CSA tensor in the molecular frame, the order parameter for the molecular ordering with respect to the distorted cages, and the order parameter for the ordering of the distorted cages with respect to the liquid crystal director. This term therefore has the form

$$\sigma_{\mathrm{RCSA}}^{\mathrm{intra}} \sim \sigma_{\mathrm{CSA}}^{\mathrm{intra}} d_{00}^2(\beta_{\mathrm{PM}}^{\mathrm{CSA}}) S_{\mathrm{MC}}^2 S_{\mathrm{CD}}^2 \qquad (16)$$

by analogy with the RDC term. Here $\beta_{\mathrm{PM}}^{\mathrm{CSA}}$ is the angle between the major principal axis of the CSA tensor and the z-axis of the molecular frame, and the intramolecular CSA tensor is assumed to have a magnitude $\sigma_{\mathrm{CSA}}^{\mathrm{intra}}$.

The likely magnitude of the intramolecular RCSA may be estimated in the case of $H_2O@C_{60}$. The proton CSA tensors of immobilized water molecules are defined by the parameters $\sigma_{\mathrm{CSA}}^{\mathrm{intra}} \simeq -6.3$ ppm and $\beta_{\mathrm{PM}}^{\mathrm{CSA}} \simeq 52^\circ$, as estimated by the solid-state NMR of gypsum[40]. Hence $d_{00}^2(\beta_{\mathrm{PM}}^{\mathrm{CSA}}) \simeq 0.069$. Since the order parameter $|S_{\mathrm{HH}}^2|$ is estimated to be 0.016 at 300 Kelvin from the RDC measurements, the order parameter product $|S_{\mathrm{MC}}^2 S_{\mathrm{CD}}^2|$ is estimated to be ~ 0.032 from equation 14. It follows that the intramolecular contribution to the RCSA is unlikely to be larger than $0.032 \times 0.069 \times 6.3$ ppm ~ 0.014 ppm. This is too small to explain the observed shifts, which are a factor of ~ 40 larger.

3. Cage-Induced RCSA. The encapsulating fullerene cages, which are postulated to have undergone a uniaxial distortion, generate an anisotropic shielding field at the site of the endohedral molecule. This leads to a contribution to the RCSA which is independent of the orientational ordering of the molecules with respect to the cage. Anisotropic shielding fields of this kind have been studied in detail for the endofullerene $H_2@C_{70}$, in which the the enclosing carbon cage has a permanent elongation[41]. The ^{19}F spectrum of $HF@C_{60}$ in the solid state also displays a signature of cage-induced CSA[3].

The cage-induced RCSA is proportional to the order parameter S_{CD}^2, but is independent of S_{MC}^2. It is expected to have the form

$$\sigma_{\mathrm{RCSA}}^{\mathrm{cage}} \sim \sigma_{\mathrm{CSA}}^{\mathrm{cage}} S_{\mathrm{CD}}^2 \qquad (17)$$

where the anisotropic shielding field from the distorted cage has a magnitude $\sigma_{\mathrm{CSA}}^{\mathrm{cage}}$, and assuming $\beta_{\mathrm{PM}}^{\mathrm{CSA(cage)}} = 0$. The two terms on the right-hand side of equation 17 are unknown. However, if we assume that the cage-induced CSA tensor $\sigma_{\mathrm{CSA}}^{\mathrm{cage}}$ is the same as that determined by the NMR of solid $H_2O@C_{60}$, which is ~ 3 ppm[15], then the order parameter for the orientation of the distorted cages in the liquid crystal would have to be $S_{\mathrm{CD}}^2 \sim 0.13$ in order to generate shifts of the observed magnitude. This is not an unreasonable value.

Unfortunately the cage-induced RCSA and magnetic susceptibility contributions to the temperature-dependent chemical shifts are in principle of similar magnitude and cannot be separated easily. For this reason we have not attempted a more detailed analysis of the ^{1}H chemical shift effects.

4.3 ^{13}C Chemical Shifts

The ^{13}C NMR spectrum of $H_2O@C_{60}$ in nematic MBBA (figure 5) shows two sharp peaks coming from the empty and filled cages. The chemical shift difference of the two peaks is ~ 0.11 ppm, which is very similar to that observed in isotropic solution[4].

This simple spectrum is not easy to reconcile with a naive interpretation of the model discussed above, in which the cages are elongated and partially aligned in anisotropic phase. The partial alignment would be expected to give a ^{13}C chemical shift contribution through the residual CSA effect. Furthermore, this contribution is expected to have opposite sign for ^{13}C sites at the "apex" of the elongated cage, as compared to ^{13}C sites at the "equator". A broadening or splitting of the ^{13}C spectrum is therefore expected.

One possible explanation for the absence of this observation is that the location of the ^{13}C sites is not stable with respect to the distorted geometry on the NMR timescale. It is plausible that the principal axes of the distortion move rapidly around the carbon cage while the carbon sites remain in place, a phenomenon known as "pseudorotation"[19]. Rapid pseudorotation averages out the residual ^{13}C CSA to zero, explaining the absence of any obvious RCSA effects in Figure 5.

5 Conclusions

In this paper we showed that the NMR of the molecular endofullerenes $H_2@C_{60}$, $H_2O@C_{60}$ and $HF@C_{60}$ dissolved in a nematic liquid crystal exhibit the signatures of partial molecular orientation. The presence of spectral splittings due to the residual dipolar coupling indicate that the endohedral molecules exhibit a weak orientational ordering with respect to the liquid crystal director. While the direct mechanism of endohedral molecule alignment cannot be ruled out, the tendency of C_{60} towards symmetry breaking[7,8,14–16] suggests that the encapsulated molecules are oriented in a three-stage process: (1) the C_{60} fullerene cages are distorted, either by interactions with the anisotropic environment of the liquid crystal, or through a mechanism intrinsic to the endofullerenes; (2) the distorted cages are partially oriented with respect to the liquid crystal director by their interactions with the oriented liquid crystal molecules; (3) the elongated cages generate an anisotropic potential for the endohedral molecules, which therefore become partially ordered with respect to the cages. We expect that a similar mechanism could be used to analyze the observed zero-field splitting effects in the EPR of $N@C_{60}$ dissolved

in a liquid crystal[17,18].

The ^{13}C observations suggest that the geometric distortion of the cage undergoes rapid pseudorotation with respect to the carbon framework.

We also intend to explore hyperpolarization effects for endohedral fullerenes in liquid crystals. Since endohedral molecules behave as quantum rotors, such hyperpolarization effects are anticipated after a temperature jump, as is observed for methyl quantum rotors[42–46]. However, quantum rotor polarization effects were not yet observed for dissolution experiments on isotropic endofullerene solutions. One possible reason for these negative results is that pairs of degenerate peaks are enhanced, but with equal and opposite amplitudes. Since the current work demonstrates the breaking of degeneracy in liquid crystal solutions, it is of interest to attempt quantum rotor hyperpolarization experiments on endofullerenes in nematic solution.

6 Acknowledgments

We thank Prof. Jim Emsley for discussions. This work was supported by EPSRC-UK (grant numbers EP/M001962/1 and EP/N002482/1).

References

1 K. Komatsu, M. Murata and Y. Murata, *Science*, 2005, **307**, 238–240.

2 K. Kurotobi and Y. Murata, *Science*, 2011, **333**, 613–616.

3 A. Krachmalnicoff, R. Bounds, S. Mamone, S. Alom, M. Concistrè, B. Meier, K. Kouřil, M. E. Light, M. R. Johnson, S. Rols, A. J. Horsewill, A. Shugai, U. Nagel, T. Rõõm, M. Carravetta, M. H. Levitt and R. J. Whitby, *Nature Chemistry*, 2016, **8**, 953–957.

4 A. Krachmalnicoff, M. H. Levitt and R. J. Whitby, *Chem. Commun.*, 2014, **50**, 13037–13040.

5 M. Xu, F. Sebastianelli, B. R. Gibbons, Z. Bacic, R. Lawler and N. J. Turro, *J. Chem. Phys.*, 2009, **130**, 224306.

6 S. Mamone, M. Ge, D. Huvonen, U. Nagel, A. Danquigny, F. Cuda, M. C. Grossel, Y. Murata, K. Komatsu, M. H. Levitt, T. RÃţÃţm and M. Carravetta, *J. Chem. Phys.*, 2009, **130**, 081103–4.

7 C. Beduz, M. Carravetta, J. Y.-C. Chen, M. Concistrè, M. Denning, M. Frunzi, A. J. Horsewill, O. G. Johannessen, R. Lawler, X. Lei, M. H. Levitt, Y. Li, S. Mamone, Y. Murata, U. Nagel, T. Nishida, J. Ollivier, S. Rols, T. Rõõm, R. Sarkar, N. J. Turro and Y. Yang, *Proc. Natl. Acad. Sci. USA*, 2012, **109**, 12894–12898.

8 M. H. Levitt, *Philos. T. Roy. Soc. A*, 2013, **371**, 20120429.

9 S. Mamone, M. JimÃľnez-Ruiz, M. R. Johnson, S. Rols and A. J. Horsewill, *Phys. Chem. Chem. Phys.*, 2016, **18**, 29369–29380.

10 A. J. Horsewill, S. Rols, M. R. Johnson, Y. Murata, M. Murata, K. Komatsu, M. Carravetta, S. Mamone, M. H. Levitt, J. Y. C. Chen, J. A. Johnson, X. Lei and N. J. Turro, *Phys. Rev. B*, 2010, **82**, 081410.

11 N. J. Turro, A. A. Marti, J. Y. C. Chen, S. Jockusch, R. G. Lawler, M. Ruzzi, E. Sartori, S. C. Chuang, K. Komatsu and Y. Murata, *J. Am. Chem. Soc.*, 2008, **130**, 10506–10507.

12 S. Mamone, M. Concistrè, E. Carignani, B. Meier, A. Krachmalnicoff, O. G. Johannessen, X. Lei, Y. Li, M. Denning, M. Carravetta, K. Goh, A. J. Horsewill, R. J. Whitby and M. H. Levitt, *J. Chem. Phys.*, 2014, **140**, 194306.

13 B. Meier, S. Mamone, M. Concistrè, J. Alonso-Valdesueiro, A. Krachmalnicoff, R. J. Whitby and M. H. Levitt, *Nature Commun.*, 2015, **6**, 8112.

14 S. Mamone, M. R. Johnson, J. Ollivier, S. Rols, M. H. Levitt and A. J. Horsewill, *Phys. Chem. Chem. Phys.*, 2016, **18**, 1998–2005.

15 M. Concistrè, S. Mamone, M. Denning, G. Pileio, X. Lei, Y. Li, M. Carravetta, N. J. Turro and M. H. Levitt, *Phil. Trans. R. Soc. A*, 2013, **371**, 20120102.

16 K. S. K. Goh, M. Jimenez-Ruiz, M. R. Johnson, S. Rols, J. Ollivier, M. S. Denning, S. Mamone, M. H. Levitt, X. Lei, Y. Li, N. J. Turro, Y. Murata and A. J. Horsewill, *Phys. Chem. Chem. Phys.*, 2014, **16**, 21330–21339.

17 C. Meyer, W. Harneit, K. Lips, A. Weidinger, P. Jakes and K.-P. Dinse, *Phys. Rev. A*, 2002, **65**, 061201(R).

18 G. Liu, M. d. C. Gimenez-Lopez, M. Jevric, A. N. Khlobystov, G. A. D. Briggs and K. Porfyrakis, *J. Phys. Chem. B*, 2013, **117**, 5925–5931.

19 C. C. Chancey and M. C. M. O'Brien, *The Jahn-Teller effect in C60 and other icosahedral complexes*, Princeton University Press, Princeton, N.J., 1997.

20 I. Haller, *Prog. Solid State Ch.*, 1975, **10**, 103–118.

21 M. L. Magnuson, B. M. Fung and J. P. Bayle, *Liq. Cryst.*, 1995, **19**, 823–832.

22 K. Takegoshi, K. Ogura and K. Hikichi, *J. Magn. Reson.*, 1989, **84**, 611–615.

23 J. A. Aguilar, M. Nilsson, G. Bodenhausen and G. A. Morris, *Chem. Commun.*, 2012, **48**, 811–813.

24 G. Pileio, S. Bowen, C. Laustsen, M. C. D. Tayler, J. T. Hill-Cousins, L. J. Brown, R. C. D. Brown, J. H. Ardenkjaer-Larsen and M. H. Levitt, *J. Am. Chem. Soc.*, 2013, **135**, 5084–5088.

25 J. W. Emsley, G. R. Luckhurst and C. P. Stockley, *Proc. R Soc. Lond. A Math. Phys. Sci.*, 1982, **381**, 117–138.

26 C. R. Sanders II, B. J. Hare, K. P. Howard and J. H. Prestegard, *Prog. Nucl. Magn. Reson. Spectrosc.*, 1994, **26, Part 5**, 421–444.

27 N. Tjandra and A. Bax, *Science*, 1997, **278**, 1111.

28 J. Prestegard, *Nature Struc. Bio.*, 1998, **5**, 492.

29 G. Cornilescu, J. L. Marquardt, M. Ottiger and A. Bax, *J. Am. Chem. Soc.*, 1998, **120**, 6836–6837.

30 H. Kneppe, V. Reiffenrath and F. Schneider, *Chemical Physics Letters*, 1982, **87**, 59–62.

31 A. Buka and W. H. De Jeu, *Journal de Physique*, 1982, **43**, 361–367.

32 P. L. Sherrell and D. A. Crellin, *Le Journal de Physique Colloques*, 1979, **40**, C3–211–C3–216.

33 M. H. Levitt, *Spin Dynamics. Basics of Nuclear Magnetic Resonance*, Wiley, Chichester, 2nd edn, 2007.

34 D. A. Varshalovich, A. N. Moskalev and V. K. Kheronskii, *Quantum Theory of Angular Momentum*, World Scientific, Singapore, 1988.
35 F. Reif and E. M. Purcell, *Phys. Rev.*, 1953, **91**, 631–641.
36 M. Tomaselli and B. H. Meier, *J. Chem. Phys.*, 2001, **115**, 11017–11020.
37 M. Tomaselli, *Mol. Phys.*, 2003, **101**, 3029–3051.
38 M. Carravetta, O. G. Johannessen, M. H. Levitt, I. Heinmaa, R. Stern, A. Samoson, A. J. Horsewill, Y. Murata and K. Komatsu, *J. Chem. Phys.*, 2006, **124**, 104507.
39 R. Seydoux, O. Muenster and P. Diehl, *Molecular Crystals and Liquid Crystals Science and Technology. Section A. Molecular Crystals and Liquid Crystals*, 1994, **250**, 99–108.
40 C. L. McKnett, C. R. Dybowski and R. W. Vaughan, *J. Chem. Phys.*, 1975, **63**, 4578–4581.
41 S. Mamone, M. Concistrè, I. Heinmaa, M. Carravetta, I. Kuprov, G. Wall, M. Denning, X. Lei, J. Y. C. Chen, Y. Li, Y. Murata, N. J. Turro and M. H. Levitt, *ChemPhysChem*, 2013, **14**, 3121–3130.
42 J. Haupt, *Phys. Lett. A*, 1972, **38**, 389–390.
43 C. Ludwig, M. Saunders, I. Marin-Montesinos and U. L. GÃijnther, *Proc. Natl. Acad. Sci. USA*, 2010, **107**, 10799–10803.
44 M. Icker and S. Berger, *J. Magn. Reson.*, 2012, **219**, 1–3.
45 B. Meier, J.-N. Dumez, G. Stevanato, J. T. Hill-Cousins, S. S. Roy, P. Håkansson, S. Mamone, R. C. D. Brown, G. Pileio and M. H. Levitt, *J. Am. Chem. Soc.*, 2013, **135**, 18746–18749.
46 J.-N. Dumez, P. Håkansson, S. Mamone, B. Meier, G. Stevanato, J. T. Hill-Cousins, S. S. Roy, R. C. D. Brown, G. Pileio and M. H. Levitt, *J. Chem. Phys.*, 2015, **142**, 044506.